The Astrophysical Journal, 1010:8 (13pp), 2026 October 10 https://doi.org/10.3847/1538-4357/aea403
© 2026. The Author(s). Published by the American Astronomical Society.
OPEN ACCESS

On Modeling the 2017 Galactic Cosmic-Ray Depression

O. P. M. Aslam[1], D. MacTaggart[2,1], M. S. Potgieter[3], M. D. Ngobeni[4], and I. I. Ramokgaba[5,6]
[1] School of Mathematics and Statistics, University of Glasgow, Glasgow G12 8QQ, UK
[2] Department of Physics, University of Trento, Povo, Italy; david.mactaggart@glasgow.ac.uk
[3] Institute for Experimental and Applied Physics (IEAP), Christian-Albrechts-University of Kiel, Kiel, Germany
[4] Department of Physical and Earth Sciences, Sol Plaatje University, Kimberley, South Africa
[5] School of Physical and Chemical Sciences, North–West University, Mmabatho, South Africa
[6] Centre for Space Research, North–West University, Potchefstroom, South Africa
Received 2026 July 14; revised 2026 August 27; accepted 2026 September 4; published 2026 October 1

Abstract

In the second half of 2017, as Solar Cycle 24 approached its minimum, a pronounced and rigidity-dependent depression in the Galactic cosmic-ray (GCR) proton flux was observed using AMS-02. This event was driven by a sequence of strong coronal mass ejections (CMEs). In this work, we model the modulation of GCR protons during this period using a steady-state Parker transport framework with parameters constrained by AMS-02 observations. Treating the event as a purely long-term modulation interval yields excellent agreement with the observed proton intensities, but implies an inferred rigidity dependence of particle mean free paths that is inconsistent with basic turbulence theory, corresponding to an effective inversion of the scattering regime. We argue that this behavior arises from the ability of highly flexible transport parameterizations to reproduce integrated modulation signatures through correlated adjustments of diffusion coefficients during transient events. To address this inconsistency, we relax the commonly adopted assumption of a time-independent ratio of perpendicular-to-parallel diffusion coefficients and introduce a physically motivated reduction of this ratio during the CME-dominated interval. This modification preserves the quality of the spectral fits while restoring the expected rigidity ordering of mean free paths. Our results indicate that allowing the perpendicular-to-parallel diffusion ratio to vary in time provides an effective means of constraining transport solutions during the 2017 depression and may help to resolve similar inconsistencies reported in other GCR modulation studies.

Unified Astronomy Thesaurus concepts: Cosmic rays (329); Heliosphere (711); Solar storm (1526)

1. Introduction

Galactic cosmic rays (GCRs) that enter the heliosphere are modulated by solar activity (M. S. Potgieter 2013a). The clearest signature of this modulation is that of the solar cycle, in which GCR flux behaves in an antiphase manner with respect to the solar cycle, i.e., the GCR flux peaks at solar minimum and troughs at solar maximum. In the second half of 2017, more specifically from 2017 June 23 to December 3 (Carrington rotations (CRs) CR2192—CR2198), the Alpha Magnetic Spectrometer (AMS-02; M. Aguilar et al. 2021a), located on the International Space Station, revealed a large and trend-reversing depression in the GCR proton (p) flux for a range of different rigidity bins (M. Aguilar et al. 2021b). This was a period when Solar Cycle 24 was approaching its minimum. The expected conditions were disturbed, however, by the presence of a highly active magnetic source on the Sun, producing a series of strong flares and coronal mass ejections (CMEs), which persisted for five solar rotations, with active region (AR) labels AR12665 → AR12670 → AR12673 → AR12682 → AR12685 (for more details, see O. P. M. Aslam et al. 2025). The production of strong flares and CMEs as the cycle approaches a minimum is a feature that has also been observed for other solar cycles (e.g., B. Tan et al. 2025). From the perspective of understanding GCR modulation, this activity poses interesting questions about how to model GCR transport. In particular, what are the consequences of an interval of high solar activity during what are otherwise conditions close to those of solar minimum?

Although not focusing on the 2017 GCR depression per se, several works have studied GCR modulation across longer periods that include the depression. O. P. M. Aslam et al. (2023) reconstruct the modulation of GCR protons and antiprotons from 2006 to 2019. To study long-term modulation effects, they make use of a well-tested steady-state model (M. S. Potgieter 2017), which captures modulation behavior on a minimum timescale of one Carrington (or Bartels) rotation and is suitable for long-term modulation studies. The model results of O. P. M. Aslam et al. (2023) clearly show the 2017 GCR depression for both protons and antiprotons. The parameterization of the model is constructed based on fitting data from AMS-02 and PAMELA (M. Aguilar et al. 2018, 2021b; O. Adriani et al. 2013; M. Martucci et al. 2018). C. Corti (2023), employing a similar steady-state transport model combined with a neural-network-accelerated parameter exploration algorithm, reports results that highlight potential physical inconsistencies in the inferred rigidity dependence of transport coefficients during the declining phase of the cycle. In particular, their work suggests that model parameterizations capable of reproducing observed intensities may imply an inverted effective rigidity dependence of scattering, in apparent tension with standard expectations from basic turbulence theory. Time-dependent modeling efforts have revealed similar behavior (e.g., X. Song et al. 2021, during the solar minimum of Cycle 24), indicating that this issue is not solely a consequence of steady-state assumptions.

Original content from this work may be used under the terms of the Creative Commons Attribution 4.0 licence. Any further distribution of this work must maintain attribution to the author(s) and the title of the work, journal citation and DOI.

The purpose of this work is not to introduce a new cosmic-ray modulation model, but to examine the physical consistency of standard long-term modulation parameterizations when applied to midterm, CME-dominated intervals, thus providing a physically consistent description of the modulation of GCR protons during the 2017 depression. We show that treating this event as a purely long-term modulation episode yields good agreement with AMS-02 intensities, but implies an inferred rigidity dependence of particle mean free paths (MFPs) that is difficult to reconcile with basic expectations from turbulence theory, resulting in similar issues found by C. Corti (2023) and X. Song et al. (2021). We argue that this behavior reflects the nonlinearity of the model, rather than evidence for unusual or inverted heliospheric turbulence. In particular, the nonlinear model supports different parameterizations that can match the observational data.

Motivated by the hybrid nature of the 2017 depression (as a period of intense solar activity between near-solar-minimum conditions), we relax the commonly adopted assumption of a time-independent ratio of perpendicular-to-parallel diffusion coefficients (DCs). By allowing this ratio to decrease during the CME-dominated depression, we obtain transport solutions that preserve agreement with AMS-02 observations while restoring the physically consistent rigidity ordering of the MFPs. This modification acts as a physically motivated constraint on the solution space, limiting compensating parameter adjustments that can otherwise mask inconsistent transport behavior in events like the 2017 depression. The results suggest that introducing time variability in the perpendicular-to-parallel diffusion ratio may provide a useful diagnostic and corrective approach for interpreting similar modulation intervals reported in recent studies.

The paper is structured as follows. In Section 2 we summarize the elements of the transport model and the parameterizations employed. Section 3 presents results obtained by modeling the 2017 depression using a conventional long-term modulation approach and highlights the resulting physical inconsistency. In Section 4, we introduce the hybrid-interval parameterization and demonstrate how it restores physically consistent transport behavior. Section 5 summarizes the main conclusions and discusses implications for future GCR modulation studies.

2. Elements of Modeling Galactic Cosmic-Ray Modulation

The four major modulation mechanisms are outward convection by the solar wind (SW), adiabatic deceleration due to the expanding SW (adiabatic cooling), diffusion along and across the heliospheric magnetic field (HMF), and drifts related to the gradient and curvature of the HMF and the heliospheric current sheet (HCS). These modulation processes are responsible for altering the differential intensities of cosmic rays as a function of energy, position, and time, and were first combined by E. N. Parker (1965) into a comprehensive transport equation (see also L. J. Gleeson & W. I. Axford 1967). The basic transport equation follows from the equation of charged particle motion in large- and small-scale fluctuating magnetic fields, and averages over the pitch and phase angles of particle propagation, with the assumption that GCRs are approximately isotropic. Within a heliocentric spherical coordinate system that rotates with the Sun, the time-dependent transport equation, incorporating explicit drift (J. R. Jokipii et al. 1977), is given by

$$\underbrace{\frac{\partial f}{\partial t}}_{(a)} = \underbrace{-\boldsymbol{v}_{\rm sw}\cdot\nabla f}_{(b)} - \underbrace{\langle \boldsymbol{v}_{\rm d}\rangle\cdot\nabla f}_{(c)} + \underbrace{\nabla\cdot(\boldsymbol{K}_{\rm s}\cdot\nabla f)}_{(d)} + \underbrace{\frac{1}{3}(\nabla\cdot\boldsymbol{v}_{\rm sw})\frac{\partial f}{\partial \ln p}}_{(e)} + \underbrace{Q}_{(f)}, \quad (1)$$

where $f(\boldsymbol{r}, p, t)$ is the omnidirectional GCR distribution function, where p is the magnitude of the particle momentum, t is time, and $\boldsymbol{r}$ is the position vector in 3D with coordinates (r, θ, ϕ) specified in a heliocentric spherical coordinate system where the equatorial plane is at a polar angle of $\theta = 90°$.

In Equation (1), the individual terms are (a) time-dependent changes in the GCR distribution function; (b) outward convection caused by the radially expanding SW, with velocity $\boldsymbol{v}_{\rm sw}$, within the corotating frame; (c) GCR gradient and curvature drift motions in the global HMF in terms of the averaged pitch-angle guiding center drift velocity $\langle \boldsymbol{v}_{\rm D}\rangle$; (d) spatial diffusion caused by the irregular HMF through the symmetric diffusion tensor $\boldsymbol{K}_{\rm s}$; (e) adiabatic energy changes (deceleration or acceleration) determined by the SW divergence $\nabla\cdot\boldsymbol{v}_{\rm sw}$ (if $\nabla\cdot\boldsymbol{v}_{\rm sw} > 0$, adiabatic energy loss (cooling) occurs as is the case in most of the heliosphere, except inside the heliosheath where we assume that $\nabla\cdot\boldsymbol{v}_{\rm sw} = 0$; see also U. W. Langner et al. 2006); and (f) possible additional sources of cosmic rays within the heliosphere (e.g., Jovian electrons). The heliosheath in the model is the region between the heliopause (HP), assumed to be at 122 au, and the SW termination shock (TS), which moves around with solar activity (see also R. Manuel et al. 2015). For more details about heliospheric transport processes and GCR modulation in general, there are several review papers, including M. S. Potgieter (1998), L. A. Fisk (1999), M. S. Potgieter (2013a, 2013b, 2017), and J. S. Rankin et al. (2022). In this study, we are interested in the behavior of GCRs over a period spanning several solar rotations, for which we take our minimum timescale to be a CR. We thus make the simplifications $\partial f/\partial t = Q = 0$. Doing this means that we seek the dominant balance in Equation (1) averaged over a CR. In other words, the outward convection of the SW (b) must be balanced by a combination of drift, diffusion, and adiabatic cooling ((c)–(e)) for each CR. This approach is consistent with previous modulation studies that address mid- to long-term variability using rotation-averaged parameters (O. P. M. Aslam et al. 2023; C. Corti 2023).

2.1. Diffusion

The convection process in Equation (1) is well understood and is based on the SW velocity, as described in detail by M. S. Potgieter et al. (2014). As a result of turbulent irregularities and fluctuations in the HMF, GCRs undergo diffusion in the heliosphere through a process called pitch-angle scattering, which can be described by quasi-linear theory (QLT) as introduced by J. R. Jokipii (1966). Such turbulence is generally interpreted either as waves (R. Schlickeiser 1988) or dynamical turbulence (e.g., J. W. Bieber & W. H. Matthaeus 1991), and is described by DCs that make up the elements of the tensor $\boldsymbol{K}_{\rm s} = (\kappa_{ij})$, $1 \leqslant i, j \leqslant 3$. These DCs can be determined from turbulence theory (see, e.g., K. D. Moloto & N. E. Engelbrecht 2020) or be based on the compatibility studies between numerical modulation models and cosmic-ray

observations in the heliosphere, as reviewed by M. S. Potgieter (2017).

Each DC is related to an MFP λ by

$$\kappa = \frac{v}{3}\lambda, \tag{2}$$

where v is the particle speed. For the case when κ is the drift coefficient (see below for details), λ is referred to as the drift scale (λ_D).

In the context of our steady-state approach, the DCs, MFPs, etc., should be interpreted as effective, Carrington-averaged transport parameters rather than instantaneous or local turbulence quantities. They, therefore, encapsulate the cumulative influence of transient disturbances, such as CMEs, on GCR transport over the averaging interval, rather than directly representing microscopic coefficients.

2.1.1. Parallel Diffusion

To model the parallel (to the magnetic field) DC, we follow previous work (e.g., M. S. Potgieter et al. 2014) in adopting a rigidity-dependent expression that has been found to be a good approximation to QLT. For its spatial dependence, the parallel DC, $\kappa_\parallel$, is considered to be inversely proportional to the HMF magnitude. The general expression used in our study to describe it is given by

$$\kappa_\parallel = \kappa_{\parallel 0}\beta\frac{B_0}{B_m}\left(\frac{P}{P_0}\right)^{c_1} \times \left[\frac{\left(\frac{P}{P_0}\right)^{c_3}+\left(\frac{P_k}{P_0}\right)^{c_3}}{1+\left(\frac{P_k}{P_0}\right)^{c_3}}\right]^{\frac{c_{2\parallel}-c_1}{c_3}}, \tag{3}$$

where P is the rigidity, B_m is the magnitude of the modified HMF (see below for further details), $\beta = v/c$ (c is the speed of light), and $\kappa_{\parallel 0}$ is a scaling constant in units of $10^{22}\,\mathrm{cm^2\,s^{-1}}$, with the rest of the equation written to be dimensionless, with $P_0 = 1.0$ GV, and $B_0 = 1.0$ nT, in order to preserve the units in $\mathrm{cm^2\,s^{-1}}$. Furthermore, c_1, $c_{2\parallel}$, and c_3 are dimensionless; c_1 is a power-law index that may change with time; $c_{2\parallel}$ and c_1 determine the slope of the rigidity dependence, respectively, above and below a rigidity with the value P_k, which may also change with time; and c_3 determines the smoothness of the transition. The rigidity dependence of $\kappa_\parallel$ is thus a combination of two power laws, where P_k determines the rigidity where the transition in the power laws occur and the value of c_1 determines the slope of the power law at rigidities below P_k.

2.1.2. Perpendicular Diffusion

The scattering of GCRs perpendicular to the HMF can be caused either as a result of the particles' gyrocenters being displaced transversely relative to the mean HMF through scattering, or due to the random walk of the magnetic-field lines themselves. These processes are collectively taken into account in numerical models via the perpendicular DC, $\kappa_\perp$. The coefficient $\kappa_\perp$ may be subdivided into two possibly independent coefficients describing perpendicular diffusion in the radial, $\kappa_{\perp r}$, and polar, $\kappa_{\perp\theta}$, directions. It has also been established that $\kappa_\perp$ plays a significant role in the modulation of GCRs (e.g., S. E. S. Ferreira et al. 2000; M. S. Potgieter 2000).

In the presence of parallel diffusion, a pure field line random walk scenario gives an insufficient description of perpendicular diffusion because particles sometimes retrace their paths after they backscatter—a process that was not taken into account until the nonlinear guiding center (NLGC) theory of particle diffusion proposed by W. H. Matthaeus et al. (2003). According to this theory, the process of perpendicular diffusion is a combination of a field line random walk, backscattering from parallel diffusion, and the transfer of particles across field lines due to the perpendicular complexity of the magnetic field (see also J. W. Bieber et al. 2004). This theory for perpendicular diffusion was later improved by A. Shalchi (2006), who proposed an extended NLGC (ENLGC), followed by a unified NLGC (UNLGC) theory in A. Shalchi (2010). For overviews of nonlinear GCR diffusion theories and comparisons with observations, the reader is directed to A. Shalchi (2009), C. Pei et al. (2010), and N. E. Engelbrecht et al. (2022).

According to the NLGC approach, perpendicular MFPs are calculated using parallel MFPs. In our work, for rigidities above P_k, $\kappa_\perp$ is scaled with a slightly weaker dependence compared to $\kappa_\parallel$, which, after converting to MFPs, results in a nonconstant $\lambda_\perp/\lambda_\parallel$ ratio (e.g., A. Shalchi et al. 2004; C. Pei et al. 2010). This translates to using different values for c_2 in Equation (3), namely $c_{2\parallel}$ for $\kappa_\parallel$ and $c_{2\perp}$ for $\kappa_\perp$.

Observations from the Ulysses spacecraft (B. Heber & M. S. Potgieter 2006, and references therein) also revealed that the latitude dependence of GCR proton fluxes is significantly weaker than predicted by classical drift models (M. S. Potgieter & L. J. Haasbroek 1993), which led J. Kóta & J. R. Jokipii (1995) to propose the concept of an anisotropic $\kappa_\perp$, where $\kappa_{\perp\theta} > \kappa_{\perp r}$ in the off-equatorial regions (see also R. A. Burger et al. 2000; M. S. Potgieter 2000).

The perpendicular DCs are given by

$$\kappa_{\perp r} = \kappa^0_{\perp r}\kappa_{\parallel 0}\beta\frac{B_0}{B_m}\left(\frac{P}{P_0}\right)^{c_1} \times \left[\frac{\left(\frac{P}{P_0}\right)^{c_3}+\left(\frac{P_k}{P_0}\right)^{c_3}}{1+\left(\frac{P_k}{P_0}\right)^{c_3}}\right]^{\frac{c_{2\perp r}-c_1}{c_3}}, \tag{4}$$

and

$$\kappa_{\perp\theta} = f_{\perp\theta}\kappa^0_{\perp\theta}\kappa_{\parallel 0}\beta\frac{B_0}{B_m}\left(\frac{P}{P_0}\right)^{c_1} \times \left[\frac{\left(\frac{P}{P_0}\right)^{c_3}+\left(\frac{P_k}{P_0}\right)^{c_3}}{1+\left(\frac{P_k}{P_0}\right)^{c_3}}\right]^{\frac{c_{2\perp\theta}-c_1}{c_3}}, \tag{5}$$

where $\kappa^0_{\perp r}$ and $\kappa^0_{\perp\theta}$ are scaling factors that will be specified later and $f_{\perp\theta}$ is a latitude-dependent function that takes care of the anisotropy in $\kappa_{\perp\theta}$, and is given by

$$f_{\perp\theta} = A^+ \mp A^- \tanh\left[\frac{1}{\Delta\theta}(\tilde{\theta} - 90^\circ \pm \theta_F)\right]. \tag{6}$$

The terms in this equation are defined as follows: $A^+ = (d_{\perp\theta}+1)/2$, $A^- = (d_{\perp\theta}-1)/2$, $\Delta\theta = 1/8$, $\theta_F = 35^\circ$, and

$$\tilde{\theta} = \begin{cases} \theta & \text{for } \theta \geqslant 90^\circ, \\ \pi - \theta & \text{for } \theta < 90^\circ, \end{cases} \tag{7}$$

where $d_{\perp\theta}$ is a dimensionless constant that determines the enhancement factor of $\kappa_{\perp\theta}$ from its value in the equatorial plane toward the poles, with respect to $\kappa_\parallel$. In this study $d_{\perp\theta} = 6$ for all particles over the entire 2016 December–2018 January period. This choice means that the polar perpendicular diffusion $\kappa_{\perp\theta}$ can be enhanced toward the heliospheric poles by a factor of 6. For the motivation of this approach, see S. E. S. Ferreira et al. (2003), M. D. Ngobeni & M. S. Potgieter (2011), and M. S. Potgieter et al. (2015). In some cases, NLGC theory suggests a very weak, or even an independent, rigidity

dependence for $\lambda_\perp$ below $\sim$ 10 GV (e.g., C. Pei et al. 2010), which, according to the modulation model, produces excessively large modulation above $\sim$1 GV. The above modeling choices are typical of the literature (M. S. Potgieter 2013a). Later, we will discuss how some of these assumptions may need to change.

2.1.3. Spatial Dependence of the Diffusion Coefficients

The analytical model describing the Parker spiral for radial distances $r \geqslant r_\odot$ (E. N. Parker 1958), modified here to incorporate the polarity structure of the HCS (see J. R. Jokipii & B. Thomas 1981; J. Kóta & J. R. Jokipii 1983), is given by the expression

$$\boldsymbol{B} = B_0 A \left(\frac{r_0}{r}\right)^2 [1 - 2H(\theta - \theta')] \times (\boldsymbol{e}_r - \tan\psi\, \boldsymbol{e}_\phi), \quad (8)$$

where $\boldsymbol{e}_r$ and $\boldsymbol{e}_\phi$ are unit vectors in the radial and azimuthal directions, respectively; $A = \pm 1$ expresses the polarity phase of the Sun ($A > 0$: positive polarity; $A < 0$: negative polarity); B_0 is the magnitude of the HMF at the Earth (i.e., $r_0 = 1$ au); and the spiral angle ψ is the angle between the radial direction and a HMF field line at any given position, defined by

$$\tan\psi = \Omega \frac{(r - R_\odot)}{|\boldsymbol{v}_{\rm sw}|} \sin\theta, \quad (9)$$

with $\Omega = 2.67 \times 10^{-6}\,{\rm rad\,s^{-1}}$ being the average angular rotation speed of the Sun. The Heaviside function H in Equation (8) determines the polarity of the magnetic field, which causes the HMF to change direction across the HCS, with θ' being the polar position of the HCS. The basic HMF structure resembles that of Archimedean spirals traversing cones of constant heliographic latitude. Beyond the position of the TS, the HMF lines are compressed as a result of the slower moving SW in the heliosheath region (see, e.g., X. Luo et al. 2024). During an $A > 0$ polarity cycle, the HMF lines will be directed outward in the northern hemisphere, and inward in the southern hemisphere (with opposite directions for an $A < 0$ cycle). In general, the spiral angle ψ in the equatorial plane at Earth is typically 45°, and increases with distance to almost 90° at $r \gtrsim 10$ au.

The magnitude of the magnetic field, from Equation (8), is given by

$$B = B_0 \left(\frac{r_0}{r}\right)^2 \sqrt{1 + (\tan\psi)^2}\,, \quad (10)$$

from which it is evident that B decreases as r^{-2} at the poles. It is known, however, that the radial magnetic field at the poles is not in perfect equilibrium due to the presence of strong turbulent convection. These motions result in transverse magnetic-field components in the polar regions, which regularly lead to deviations from the smooth Parker field geometry (J. R. Jokipii & J. Kóta 1989; R. J. Forsyth et al. 1996). While the dynamics of changes to the radial magnetic field at the poles are complex, the effects of producing a more tightly wound spiral and larger spiral angles at larger distances can be incorporated using the adjustment proposed by C. W. Smith & J. W. Bieber (1991). They suggest that Equation (9) be modified to

$$\tan\psi' = \Omega \frac{(r - R_\odot)}{|\boldsymbol{v}_{\rm sw}(r,\,\theta)|} \sin\theta \; - \frac{r|\boldsymbol{v}_{\rm sw}(r_b,\,\theta)|}{r_b|\boldsymbol{v}_{\rm sw}(r,\,\theta)|} \frac{B_T(r_b)}{B_R(r_b)}, \quad (11)$$

where B_T/B_R is the ratio of the azimuthal magnetic-field component to the radial component and r_b is some radial distance from the center of the Sun. Here, we follow J. L. Raath et al. (2016) in setting $r_b = 20\,R_\odot$ and $B_T(r_b)/B_R(r_b) \approx -0.02$. The HMF with this modification is denoted $\boldsymbol{B}_{\rm m}$ (with magnitude $B_{\rm m}$, see Equation (3)). For more details about this modification and its physical justification, the reader is directed to C. W. Smith & J. W. Bieber (1991) and J. L. Raath et al. (2016).

2.2. Particle Drifts

The significance of particle drifts, not included in the original derivation of the transport equation, was not realized until J. R. Jokipii et al. (1977) pointed out that this process might contribute to CR modulation. This was later confirmed by modulation models that included drift effects (J. Kóta & J. R. Jokipii 1983; M. S. Potgieter & H. Moraal 1985). The global background HMF induces drift motions in GCRs, which originate as a result of gradients in the HMF magnitude, the curvature of the field, and any sudden changes in the field direction, like those found at the HCS (e.g., R. A. Burger & M. S. Potgieter 1989), in addition to a charge asymmetry as a result of the sensitivity of drifts to the HMF polarity. The pitch-angle-averaged guiding center drift velocity can be written as

$$\langle \boldsymbol{v}_d \rangle = \nabla \times \kappa_A \frac{\boldsymbol{B}}{B}, \quad (12)$$

where κ_A is the global drift coefficient that is discussed below. If we write $\boldsymbol{B}/B = [1 - 2H(\theta - \theta')]\boldsymbol{e}_B$, where $\boldsymbol{e}_B$ is a unit vector parallel to $\boldsymbol{B}$, we can reexpress Equation (12) as

$$\begin{aligned} \langle \boldsymbol{v}_{\rm d} \rangle &= [1 - 2H(\theta - \theta')] \nabla \times \kappa_A \boldsymbol{e}_B \\ &\quad + \frac{2\kappa_A}{r} \delta(\theta - \theta') \boldsymbol{e}_B \times \boldsymbol{e}_\theta \\ &= [1 - 2H(\theta - \theta')] \langle \boldsymbol{v}_{\rm d} \rangle_{\rm gc} \\ &\quad + \delta(\theta - \theta') \langle \boldsymbol{v}_{\rm d} \rangle_{\rm HCS}, \end{aligned} \quad (13)$$

where $\langle \boldsymbol{v}_{\rm d} \rangle_{\rm gc}$ represents the average drift velocity due to gradients and curvature in the HMF and $\langle \boldsymbol{v}_{\rm d} \rangle_{\rm HCS}$ represents the average drift velocity due to current sheet drift because of a switch in magnetic polarity over the HCS. The derivative of the Heaviside function leading to the delta function in Equation (13) is taken in the sense of distributions.

When modeling the drift velocity, we follow previous work (R. A. Burger et al. 2000; M. D. Ngobeni & M. S. Potgieter 2015; J. L. Raath et al. 2016) and write

$$\kappa_A = \kappa_{A0} \frac{\beta P}{3B_{\rm m}} \frac{(P/P_{A0})^2}{1 + (P/P_{A0})^2}, \quad (14)$$

where $\kappa_{A0} \in [0, 1]$ is a dimensionless constant parameterizing the amount of drift reduction due to diffusive scattering and P_{A0} (in GV units) is a quantity added on dimensional grounds. Equation (14) represents a deviation from weak scattering, with particles with rigidity below P_{A0} having drifts that are progressively reduced with respect to the weak scattering case

Table 1
Summary of the Calculated Intrinsic and Modulation Parameters Used to Reproduce Proton Observations for the Period 2016 December 14 (CR2185) to 2018 January 26 (CR2199)

Time	HMF (nT)	α (deg)	$d_{\rm TS}$ (au)	$\kappa_{\parallel 0}$	κ_{A0}	P_{A0} (GV)	c_1	$c_{2\parallel}$	$c_{2\perp r}$ (% $c_{2\parallel}$)	$c_{2\perp\theta}$ (% $c_{2\parallel}$)	c_3	P_k (GV)	$d_{\perp\theta}$
CR2185	6.11	26.72	83.0	66.95	0.90	0.90	1.11	1.60	0.66	0.65	2.50	2.90	6.0
CR2186	6.00	25.87	82.50	68.61	0.90	0.90	1.05	1.60	0.66	0.65	2.50	3.0	6.0
CR2187	5.94	24.92	82.50	70.63	0.90	0.90	1.01	1.60	0.66	0.65	2.50	3.10	6.0
CR2188	5.83	23.53	82.50	70.77	0.90	0.90	0.96	1.60	0.66	0.65	2.50	3.20	6.0
CR2189	5.74	22.49	82.0	69.59	0.90	0.90	0.96	1.60	0.66	0.65	2.50	3.00	6.0
CR2190	5.70	21.80	82.0	72.30	0.90	0.90	0.96	1.60	0.66	0.65	2.50	3.10	6.0
CR2191	5.64	21.19	82.0	72.44	0.90	0.90	0.94	1.58	0.66	0.65	2.50	3.30	6.0
CR2192	5.56	20.56	82.0	70.77	0.90	0.90	0.92	1.58	0.65	0.65	2.50	3.30	6.0
CR2193	5.31	19.48	81.50	63.89	0.90	0.90	0.92	1.58	0.65	0.65	2.50	3.0	6.0
CR2194	5.30	18.99	81.50	62.91	0.90	0.90	0.92	1.58	0.65	0.65	2.50	3.0	6.0
CR2195	5.27	18.66	81.50	60.13	0.90	0.90	0.90	1.58	0.66	0.65	2.50	2.80	6.0
CR2196	5.29	18.05	81.50	65.00	0.90	0.90	0.90	1.60	0.665	0.65	2.50	2.70	6.0
CR2197	5.29	17.34	81.50	70.56	0.90	0.90	0.89	1.60	0.665	0.65	2.50	2.80	6.0
CR2198	5.28	16.29	81.0	73.00	0.90	0.90	0.88	1.60	0.665	0.65	2.50	2.80	6.0
CR2199	5.24	15.31	81.0	74.79	0.90	0.90	0.88	1.60	0.665	0.65	2.50	2.80	6.0

Note. Time is displayed by CR number, CR2185 (2016 December 14–2017 January 09) to CR2199 (2017 December 30–2018 January 26). The distance to the TS is denoted $d_{\rm TS}$. All other parameters are defined in the main text.

(in the weak scattering limit, $\kappa_A \rightarrow \kappa_{A0}\beta P/(3B_{\rm m})$). For more details of the properties of Equation (14) and its relation to observations, we direct the reader to M. S. Potgieter (2013a) and references within.

2.3. Very Local Interstellar Spectrum

The very local interstellar spectrum (vLIS) describes the spectrum of protons at the edge of the heliosphere, which we take to be 122 au. All modulations results relate to how the proton spectrum changes relative to the vLIS. In this work, we use the same vLIS as that of O. P. M. Aslam et al. (2023), which, following D. Bisschoff et al. (2019), has the form

$$J_p(\Gamma) = \frac{2620}{\beta^2}\Gamma^{1.1}\left(\frac{\Gamma^{0.98}+0.7^{0.98}}{1+0.7^{0.98}}\right)^{-4} + 30\Gamma^2\left(\frac{\Gamma+8}{9}\right)^{-12}, \quad (15)$$

where J_p is the GCR intensity (with units of particles $\rm m^{-2}\,s^{-1}\,sr^{-1}\,(GV\,nuc^{-1})^{-1}$) and $\Gamma = E/E_0$ where E is the kinetic energy (units of $\rm GV\,nuc^{-1}$), where $E_0 = 1\,\rm GV\,nuc^{-1}$. For an overview, see M. S. Potgieter et al. (2021) and references therein.

3. Model 1: A Long-term Modeling Approach

The transport framework described in Section 2 has been shown to successfully reproduce GCR modulation over a complete solar cycle (e.g., O. P. M. Aslam et al. 2023). As a starting point, we therefore apply this long-term modulation approach to the 2017 depression, treating the event in the same manner as other intervals within the declining phase of Solar Cycle 24. This approach provides a well-defined baseline against which the physical consistency of the resulting transport solutions can be assessed.

We emphasize that the purpose of this section is not merely to reproduce the AMS-02 observations which, as shown below, can be achieved to high precision, but to examine whether a conventional parameterization for long-term modulation yields transport behavior that remains physically consistent when applied to a midterm event like the 2017 depression. As will be demonstrated, although this approach accurately captures the observed proton intensities, it leads to an inferred rigidity dependence of particle MFPs that deviates significantly from basic turbulence theory.

We make use of the the 1 day resolution observations reported by M. Aguilar et al. (2021b) for protons. In line with O. P. M. Aslam et al. (2023), we fix the parameters $\kappa_{A0} = 0.9$ and $P_{A0} = 0.9$ GV in Equation (14). The first of these relates to the drift coefficient corresponding to a 90% weak scattering gradient and curvature drifts. For the second parameter, this describes a cutoff rigidity, below which there is greater deviation from weak scattering. We set $\kappa^0_{\perp r} = \kappa^0_{\perp\theta} = 0.02$, which is a common assumption in many previous works (including X. Song et al. 2021; O. P. M. Aslam et al. 2023; C. Corti 2023). The parameter c_3 is also fixed.

For each CR considered, the code is run iteratively by varying the model parameters until the rms value, across the rigidity and time ranges considered, of the percentage difference between the model and observational differential intensities is less that 5%. As will be shown later, this approach results in rms values lower than this threshold and the greatest percentage difference at a particular CR is less than 7%.

Given the above model assumptions, and fitting the model to match differential intensity spectra data from AMS-02 (which will be displayed shortly), a full list of model parameters is displayed in Table 1.

The parameter c_1 decreases with time, which is indicative of long-term modulation. The remaining parameters in Table 1 vary with time in a nonmonotonic fashion, which is necessary in order to reproduce the observed behavior of the 2017 GCR depression. While some parameters, like $\kappa_{\parallel 0}$, exhibit minima that correspond to the minimum of the depression, it is important to take into account nonlinear relations with other parameters, such as P_k and the c powers for diffusion, in order to develop a complete understanding of the key underlying

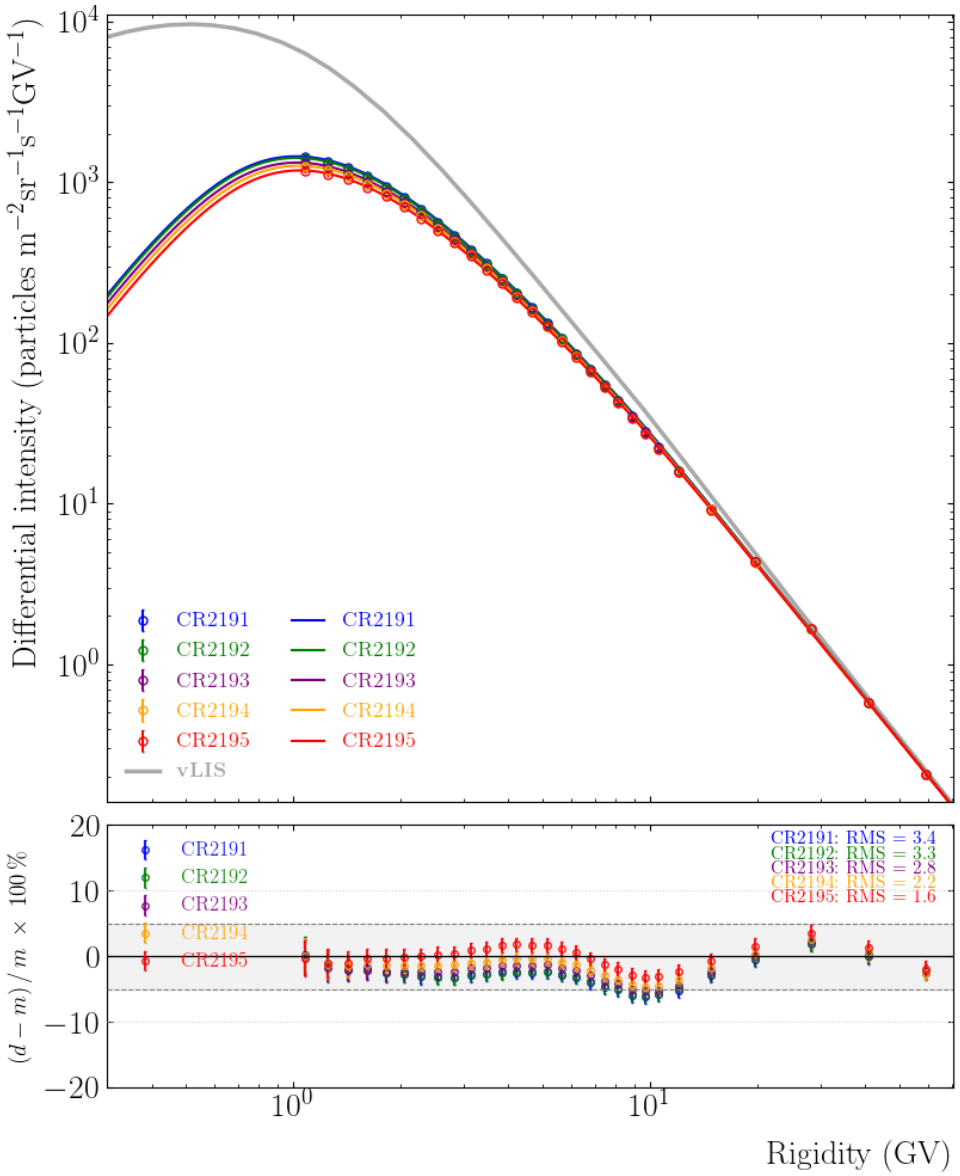


Figure 1. Differential Intensity of Galactic protons at Earth (1 au) during the CR2191–CR2195. The lines are model results and circles are AMS-02 observations adopted from M. Aguilar et al. (2021b). The gray line shows the shape of vLIS. The accuracy of the model fit is shown below where the relative percentage difference between the data (d) and the model (m). The rms errors per CR are also highlighted.

physics. For the period under study, the Sun was in a positive HMF polarity phase ($A > 0$). Thus, for protons, we set $A = 1$.

3.1. Differential Intensity and Flux Variation

Based on the above parameterization, Figure 1 shows the modeled differential intensity spectra of GCR protons at the Earth for CR2191–CR2195, together with AMS-02 observations. The corresponding vLIS is shown for reference. The parameter values listed in Table 1 are chosen to reproduce the observed spectral shapes and differential intensities across the full range of measured rigidities.

At lower rigidities, where observational data are not available, the shape of the differential intensity spectra at the Earth is influenced by the fact that protons are highly susceptible to adiabatic cooling, which is the reason for the steady slopes of these modulated spectra (see also M. D. Ngobeni et al. 2020). For observational evidence of this behavior, see, for example, M. Martucci et al. (2018).

The temporal evolution of the proton flux for the lowest-rigidity bin measured by AMS-02 is shown in Figure 2. The model accurately reproduces both the timing and magnitude of the depression, as well as the subsequent recovery toward near-minimum conditions. This agreement highlights the ability of the long-term modulation framework to capture the integrated impact of the transient CME activity on the observed proton fluxes. In this sense, the model performs at least as well as previous steady-state and time-dependent approaches applied to this interval.

In the model, we can also experiment with how changing a particular part of the physics affects the modulation profile. For example, if we fix $\kappa_{\parallel 0} = 72.44$, i.e., the value just before the depression, and maintain this value from CR2191 to CR2199, while keeping all other values in Table 1 as before, the result is indicated by the red line in Figure 2. Essentially, the proton flux continues its recovery toward solar minimum modulation as if there were no CMEs disturbing it. This is a

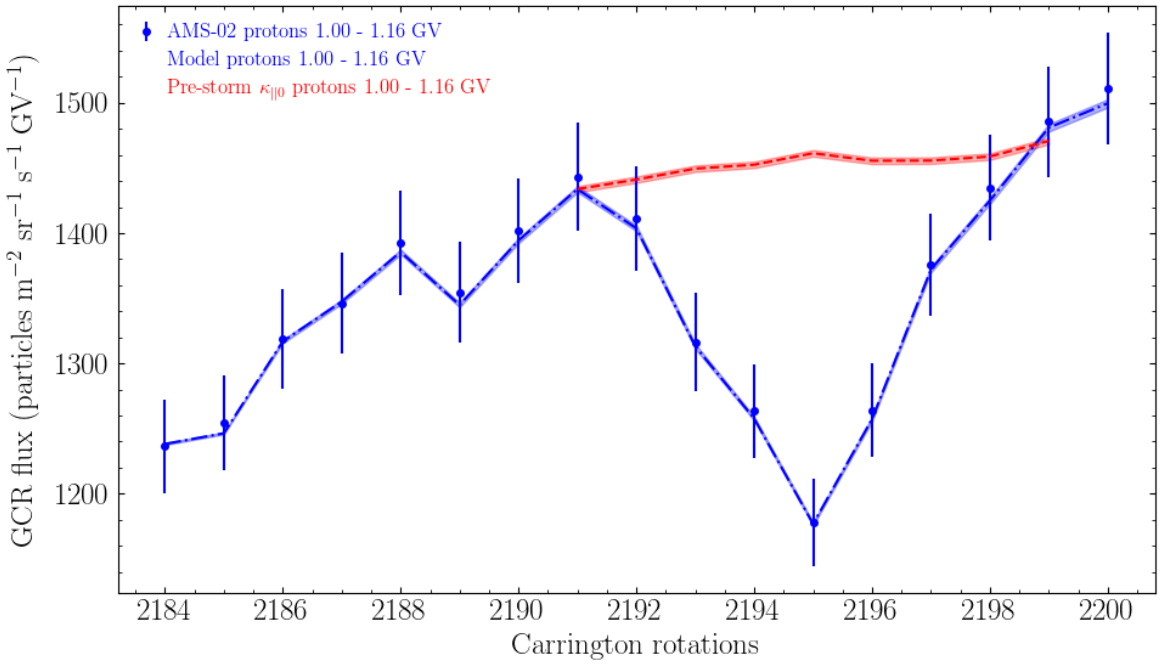


Figure 2. Time variation of modeled Galactic proton flux for the rigidity range 1.0–1.16 GV along with standard error of mean (SEM; =standard deviation $\sigma/\sqrt{n}$) as shading around solid line, here compared with corresponding AMS-02 observations of the same rigidity range for the time period CR2184–CR2200. The meaning of the red dashed line is discussed in the main text.

test of the model's consistency as this behavior is what would be expected if there were no CMEs—there would be no disturbance due to the CMEs and thus no depression. This result further highlights the importance of varying a quantity like $\kappa_{\|0}$ in time, in addition to changing the HMF magnitude and the HCS tilt angle.

However, it is important to emphasize that the quality of the spectral and temporal fits alone does not uniquely constrain the underlying transport physics. The modulation profile primarily reflects the net effectiveness of competing transport processes acting over the heliosphere, allowing correlated adjustments of DCs and rigidity dependences to compensate for one another. As a result, transport parameterizations can reproduce the observed intensities even when the implied rigidity dependence of particle scattering deviates from standard physical expectations. To assess whether the long-term parameterization (in Table 1) yields physically consistent transport behavior during this transient event, it is therefore necessary to examine the inferred rigidity dependence of the diffusion and drift scales in more detail.

3.2. Mean Free Paths and Drift Scales

As discussed above, the rigidity dependence of diffusion MFPs and drift scales plays a central role in determining the modulation of GCRs. To examine the physical implications of the long-term modulation parameterization, Figure 3 shows the rigidity dependence of the parallel MFP $\lambda_{\|}$, the perpendicular MFPs $\lambda_{\perp r}$ and $\lambda_{\perp\theta}$, and the drift scale λ_{D} at Earth for selected CRs spanning the 2017 depression. The functional forms of the quantities displayed in Figure 3, as well as their numerical values, are similar to those of O. P. M. Aslam et al. (2023).

The corresponding temporal evolution of the parallel and (radial) perpendicular MFPs for a range of rigidities is shown in Figure 4.

During the development of the depression, Figure 4 reveals that the relative reduction of MFPs is stronger for higher-rigidity protons than for lower-rigidity protons. In particular, the parallel and radial perpendicular MFPs at higher rigidities decrease more sharply through the onset and peak of the depression. This behavior implies that higher-rigidity particles experience comparatively stronger modulation than lower-rigidity particles during this interval. Such a rigidity ordering corresponds to an effective scattering regime that is opposite to that expected for heliospheric turbulence dominated by large-scale fluctuations.

Under conventional assumptions, higher-rigidity particles are expected to undergo weaker resonant scattering and therefore possess larger MFPs than lower-rigidity particles. The behavior inferred from this model, therefore, challenges standard expectations and is described, in an inferred sense, as corresponding to an inverted rigidity dependence of particle scattering. We stress that this inversion is not a direct measurement of the heliospheric magnetic-field power spectrum, but rather a diagnostic implication arising from the fitted rigidity dependence of the transport coefficients within the adopted modulation framework.

Importantly, this inferred inversion occurs despite the excellent agreement between modeled and observed proton intensities demonstrated in Figures 1 and 2. This apparent contradiction can be understood in terms of dominant balance in the steady-state Parker transport equation. When averaged over a CR, the transport solution is governed by a balance between outward SW convection and a combination of diffusion, drifts, and adiabatic energy changes, as indicated in Equation (16):

$$0 \approx -\boldsymbol{v}_{\mathrm{sw}} \cdot \nabla f + \nabla \cdot [\kappa_{\|} \nabla_{\|} f + \kappa_{\perp} \nabla_{\perp} f] - \langle \boldsymbol{v}_{\mathrm{d}} \rangle \cdot \nabla f + \frac{1}{3} (\nabla \cdot \boldsymbol{v}_{\mathrm{sw}}) \frac{\partial f}{\partial \ln p}. \quad (16)$$

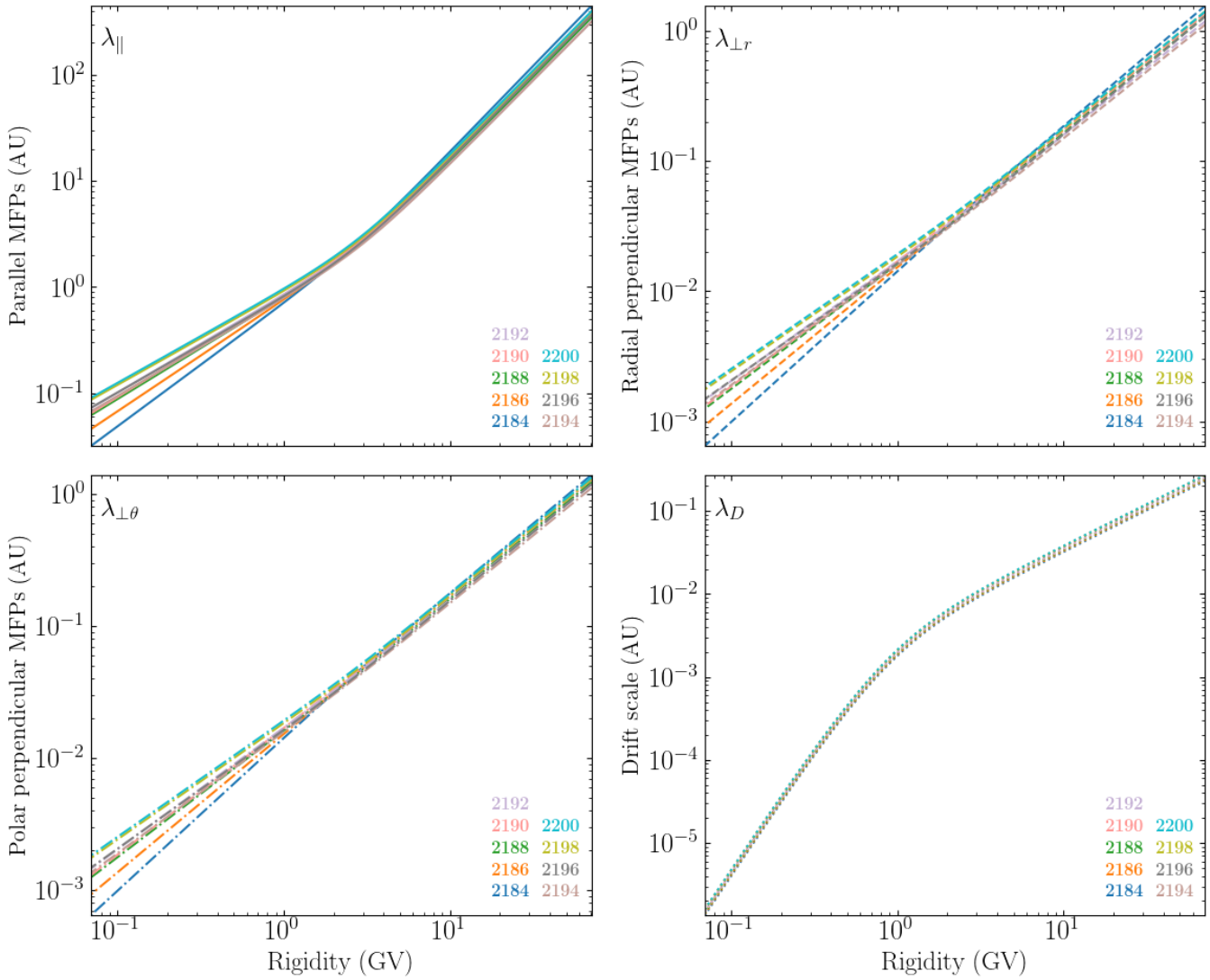


Figure 3. Rigidity dependence of the parallel ($\lambda_{\parallel}$) and two perpendicular ($\lambda_{\perp r}$, $\lambda_{\perp\theta}$) MFPs, and the drift scale (λ_D) in astronomical units for protons for alternate CRs from 2184–2200.

As a consequence, different combinations of $\kappa_{\parallel}$, $\kappa_{\perp}$, and their associated rigidity slopes (see Section 2 for more details) can satisfy the same dominant balance at a given rigidity, allowing for a physically inconsistent rigidity ordering of MFPs to persist without degrading the agreement with observed fluxes. Thus, agreement with observed intensities alone is insufficient to guarantee physically consistent rigidity-dependent transport during transient modulation events, and so motivates the need for additional physical constraints beyond goodness-of-fit considerations.

The appearance of this behavior in a long-term modulation parameterization, together with similar results reported in both steady-state and time-dependent studies (X. Song et al. 2021; C. Corti 2023), is suggestive of a limitation of commonly adopted model assumptions when applied to CME-dominated hybrid intervals, like the 2017 depression, rather than evidence for a genuine reversal of heliospheric turbulence properties. In the following section, we, therefore, explore whether relaxing one such assumption, motivated by the physical conditions of the 2017 depression, can constrain the transport solutions and restore the expected rigidity ordering of the MFPs.

4. Model 2: Adapting for "Hybrid" Conditions

The results of Section 3 demonstrate that treating the 2017 depression as a purely long-term modulation interval leads to transport solutions that reproduce the observed proton intensities but imply a physically inconsistent rigidity dependence of particle scattering. As argued above, this behavior is a consequence of the nonlinear nature of the Parker transport equation. Different combinations of diffusion and drift coefficients can produce similar modulation profiles because the observed flux reflects the net balance of several competing transport processes. Consequently, agreement with observations does not by itself guarantee that the inferred rigidity dependence of the transport parameters is physically realistic.

The purpose of this section, therefore, is not to improve the quality of the fit to the AMS-02 data, but to investigate whether an additional physically motivated constraint can reduce the degeneracy of the transport solution space and eliminate the inferred rigidity-ordering inconsistency identified in Section 3. As demonstrated by O. P. M. Aslam et al. (2025),

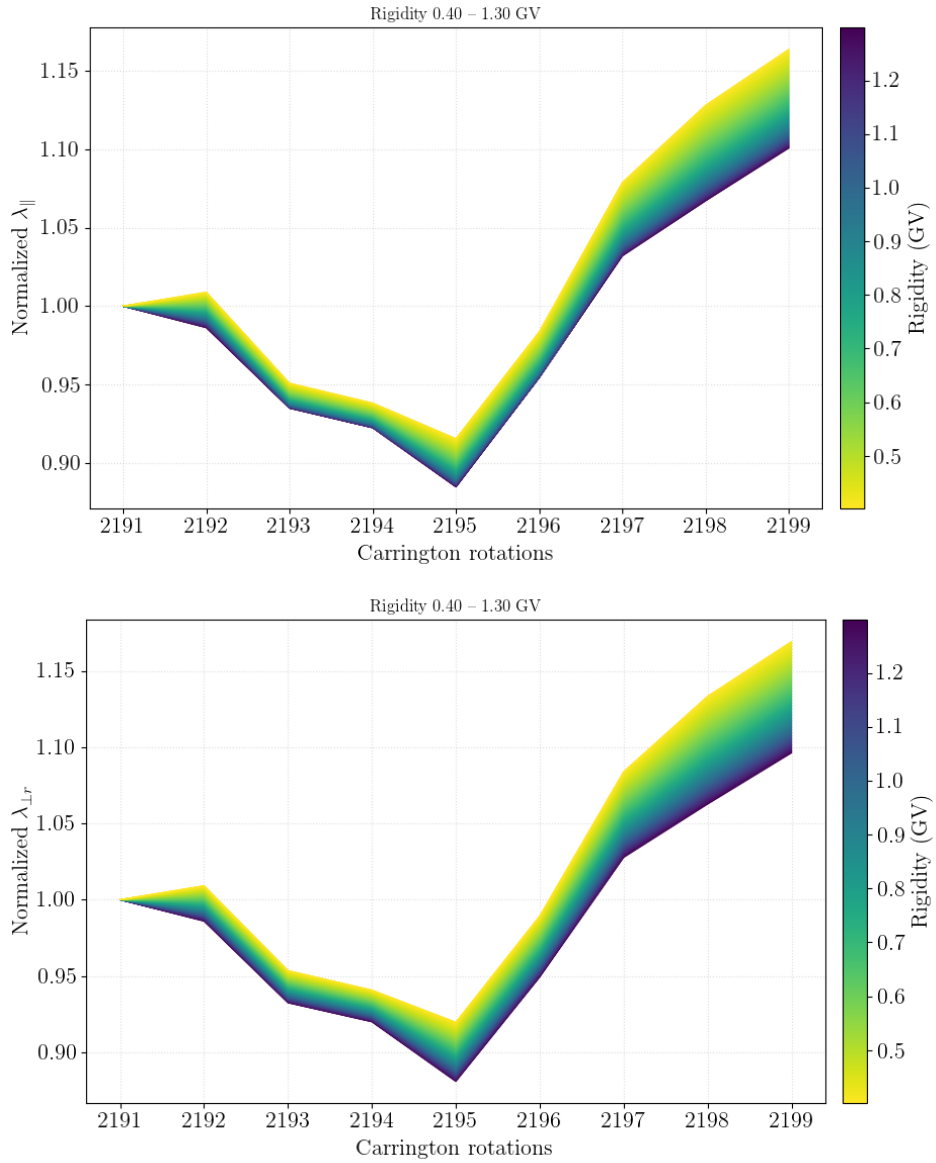


Figure 4. Time dependence in parallel ($\lambda_{\parallel}$; top) and perpendicular ($\lambda_{\perp r}$; bottom) MFPs of protons for rigidities of 0.40–1.30 GV, over the 2017 depression period CR2191–CR2198, normalized with respect to CR2191.

the interval CR2191–CR2197 was characterized by repeated CME-driven disturbances that continually interrupted the recovery of the proton flux. Such disturbances are commonly interpreted as diffusion barriers or magnetic obstacles that inhibit cosmic-ray penetration into disturbed heliospheric regions (J. A. Lockwood 1971; G. Wibberenz et al. 1998; H. V. Cane 2000; M. Dumbović et al. 2020, 2022). Since the transport coefficients used here represent effective Carrington-averaged quantities rather than instantaneous local turbulence parameters, the repeated occupation of successive CRs by strong CME-driven disturbances implies an effective transport regime that differs from that of the surrounding near-minimum heliosphere. We, therefore, investigate whether a modest reduction in the effective ratio $\kappa_{\perp r}/\kappa_{\parallel}$, motivated by the diffusion-barrier interpretation of CME-driven cosmic-ray depressions, can provide an additional physical constraint on the transport solution space and thereby eliminate the inferred rigidity-ordering inconsistency identified in Section 3.

Performing this change, we find that modifying the polar component of the perpendicular DC, $\kappa_{\perp\theta}$, has a negligible impact on the modulation results for the 2017 depression, whereas changes to the radial component, $\kappa_{\perp r}$, produce a substantial effect. This difference arises because the observed proton fluxes at the Earth are primarily sensitive to radial transport through the heliosphere, particularly during intervals dominated by outward-propagating CMEs. While enhanced polar perpendicular diffusion plays an important role in reproducing the weak latitudinal gradients observed by Ulysses and related missions, it contributes only indirectly to the radial modulation experienced by particles reaching 1 au. In contrast, $\kappa_{\perp r}$ directly controls the efficiency with which particles can diffuse across the Parker spiral field while propagating radially inward against SW convection. Consequently, reducing $\kappa_{\perp r}$ during the CME-dominated phase significantly alters the relative modulation of particles at different rigidities, suppressing compensating cross-field transport and restoring the

Table 2
Summary of the Calculated Intrinsic and Modulation Parameters (Changed Parameters Are in Bold) Used to Reproduce Proton Observations for the CR2190–CR2199

Time	HMF (nT)	α (deg)	$d_{\rm TS}$ (au)	$\kappa_{\parallel 0}$	$\kappa^0_{\perp r}$	κ_{A0} (GV)	P_{A0}	c_1	$c_{2\parallel}$	$c_{2\perp r}$ (% $c_{2\parallel}$)	$c_{2\perp\theta}$ (% $c_{2\parallel}$)	c_3	P_k (GV)	$d_{\perp\theta}$
CR2190	5.70	21.80	82.0	72.30	0.02	0.90	0.90	0.96	1.60	0.66	0.65	2.50	3.10	6.0
CR2191	5.64	21.19	82.0	**89.46**	**0.016**	0.90	0.90	**0.94**	1.58	**0.55**	0.65	2.50	3.30	6.0
CR2192	5.56	20.56	82.0	**85.88**	**0.016**	0.90	0.90	**0.93**	1.58	**0.55**	0.65	2.50	3.30	6.0
CR2193	5.31	19.48	81.50	**78.23**	**0.016**	0.90	0.90	**0.92**	1.58	**0.55**	0.65	2.50	**3.30**	6.0
CR2194	5.30	18.99	81.50	**76.78**	**0.016**	0.90	0.90	**0.955**	1.58	**0.55**	0.65	2.50	**3.30**	6.0
CR2195	5.27	18.66	81.50	**71.75**	**0.016**	0.90	0.90	**0.985**	1.58	**0.55**	0.65	2.50	**3.30**	6.0
CR2196	5.29	18.05	81.50	**78.60**	**0.016**	0.90	0.90	**0.955**	1.58	**0.55**	0.65	2.50	**3.30**	6.0
CR2197	5.29	17.34	81.50	**85.04**	**0.016**	0.90	0.90	**0.960**	1.58	**0.55**	0.65	2.50	**3.30**	6.0
CR2198	5.28	16.29	81.0	**87.76**	**0.016**	0.90	0.90	**0.965**	1.58	**0.55**	0.65	2.50	**3.30**	6.0
CR2199	5.24	15.31	81.0	74.79	0.02	0.90	0.90	0.88	1.60	0.665	0.65	2.50	2.80	6.0

expected rigidity ordering of the MFPs. We, therefore, leave $\kappa_{\perp\theta}$ at its long-term value and focus exclusively on changing $\kappa_{\perp r}$ as a minimal and physically motivated adjustment to the standard parameterization.

Table 2 summarizes the revised parameterization adopted during the CME-dominated interval CR2190–CR2198, with the parameters that differ from the long-term model highlighted in bold. Relative to Table 1, the key modification is a reduction in the normalization of the radial perpendicular DC, $\kappa_{\perp r}$, during the depression. The value $\kappa_{\perp r} = 0.016$ is the first value, steadily decreasing in increments of 0.001 from the Model 1 value of 0.02, for which there is a qualitative change in the behaviors of the MFPs relative to Model 1. All other parameters are adjusted only as required to preserve the quality of the fit to the AMS-02 proton observations which, as is clear from Figure 5, is comparable to that of Model 1.

An important consequence of reducing $\kappa_{\perp r}$ is that the parallel diffusion normalization $\kappa_{\parallel 0}$ increases during the depression relative to the long-term parameterization, while retaining its minimum near the peak of the event at CR2195. This compensating change reflects the nonlinear coupling between DCs required to maintain the observed modulation depth when cross-field transport is suppressed. At the same time, the temporal evolution of the rigidity slope parameter c_1 is no longer strictly monotonic. This behavior indicates that the 2017 depression is better characterized as a midterm modulation event, superimposed on the long-term solar-cycle trend, rather than as part of smooth secular evolution.

Despite these adjustments, the revised parameterization differs from the long-term model in a limited and controlled manner. This demonstrates that restoring physically consistent rigidity-dependent transport does not require a wholesale restructuring of the model, but can be achieved by relaxing a single simplifying assumption in a physically motivated way.

Figure 6 compares the rigidity dependence of the parallel MFPs, the perpendicular MFPs, and the drift scale for Models 1 and 2 at CR2191 and CR2195, representing the onset and peak of the 2017 depression respectively. While the rigidity dependences of $\lambda_\parallel$, $\lambda_{\perp\theta}$, and $\lambda_{\rm D}$ are broadly similar between the two parameterizations, a clearer qualitative difference is evident in the behavior of the radial perpendicular MFP $\lambda_{\perp r}$. In Model 2, $\lambda_{\perp r}$ exhibits a noticeably flatter rigidity dependence at higher rigidities, particularly at the peak of the depression, in closer agreement with expectations from basic theory (e.g., N. E. Engelbrecht et al. 2022). This contrasts with Model 1, in which $\lambda_{\perp r}$ increases more steeply with increasing rigidity, contributing to the inferred inversion of the scattering regime.

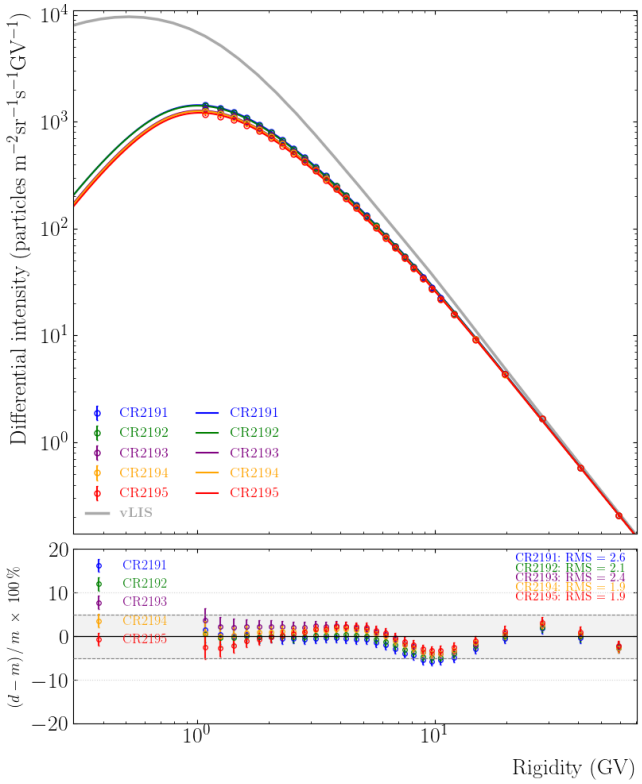


Figure 5. Model 2 results (solid lines) of the differential intensity of Galactic protons at the Earth (1 au) during CR2191–CR2195, using the new parameters for the 2017 GCR depression displayed in Table 2. AMS-02 observations (M. Aguilar et al. 2021b) are shown as circles and the vLIS is displayed as a gray line. The accuracy of the model fit is shown below where the relative percentage difference between the data (d) and the model (m). The rms errors per CR are also highlighted.

The impact of this difference becomes most apparent when examining the temporal evolution of the MFPs. Figure 7 shows the time dependence of $\lambda_\parallel$ and $\lambda_{\perp r}$ for a range of rigidities, normalized to their values at CR2191. In Model 2, lower-rigidity particles experience a more pronounced relative reduction in MFP during the development of the depression, consistent with standard modulation theory. Moreover, as the depression subsides toward CR2198, the MFPs of lower-rigidity particles recover more rapidly than those at higher rigidities, restoring the expected rigidity ordering throughout the recovery phase.

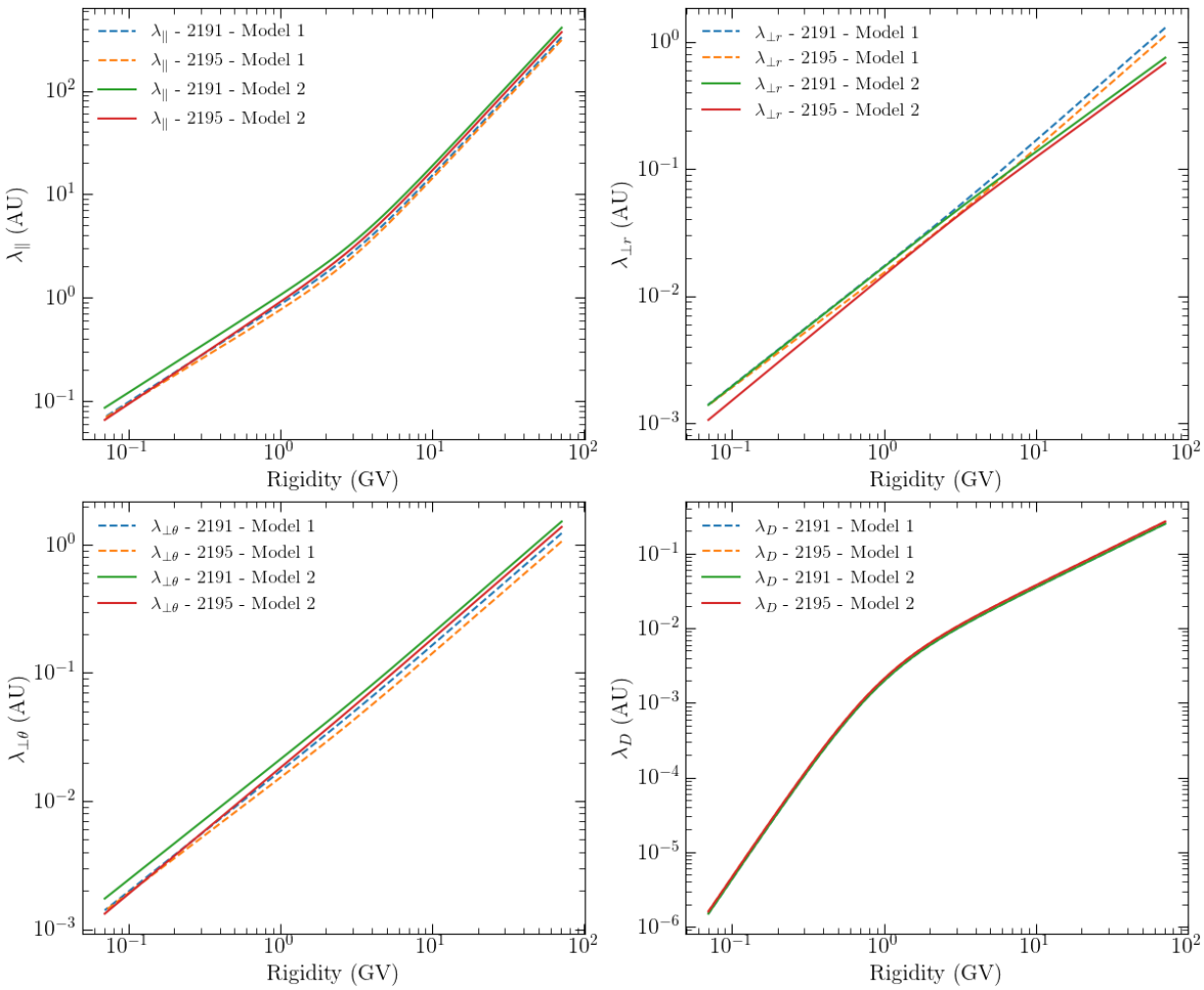


Figure 6. Rigidity dependence of MFPs and the drift scale—a comparison between Model 1 (dashed lines) and Model 2 (solid lines) for CR2191 and CR2195.

By contrast, in Model 1 (Figure 4), higher-rigidity particles exhibit stronger relative suppression through much of the depression, leading to the inferred inverted rigidity dependence discussed in Section 3.2. The comparison between Figures 4 and 7, therefore, demonstrates that allowing the perpendicular-to-parallel diffusion ratio to vary during the CME-dominated interval suppresses compensating cross-field transport and constrains the dominant balance of the transport equation in a physically consistent manner. Importantly, this improvement is achieved without degrading the agreement with the observed proton intensities, indicating that the revised parameterization restores physical consistency rather than merely reshuffling the fit.

5. Summary and Conclusions

In this work, we model the modulation of GCR proton flux during the second half of 2017, when a particularly large depression in the GCR proton flux was detected with AMS-02. We do this by applying a well-tested model (e.g., M. S. Potgieter et al. 2014; M. D. Ngobeni et al. 2022), matched to the latest AMS-02 observations of the period. We first follow the approach of O. P. M. Aslam et al. (2023) in modeling the depression as a long-term modulation event. Although we achieve a good match between the model and the observed spectra, the results lead to a physical inconsistency in which the MFPs of protons are more strongly affected for particles of higher rigidity compared to those of low rigidity. This result is consistent with an inferred rigidity dependence of particle scattering that departs from standard expectations (e.g., C. Corti 2023). To address this issue, we adapt the standard model assumption of a constant ratio of perpendicular-to-parallel diffusion tensor coefficients, $\kappa_{\perp}/\kappa_{\parallel}$, and consider a time-dependent ratio. In particular, we reduce the value of $\kappa_{\perp}/\kappa_{\parallel}$ during the depression in order to better model this "hybrid" period of CME activity during otherwise near-minimum conditions. The ratio during the depression is reduced by approximately 20% relative to its long-term value, motivated by the diffusion-barrier interpretation of CME-driven cosmic-ray depressions, while preserving agreement with the AMS-02 observations. Performing a change like this does not necessarily guarantee a physically consistent solution but it does represent a physically motivated approach to improving the model.

The effect of this small change is substantial on the model results. The new parameterization leads to a physically consistent solution, i.e., the MFPs recover the physically expected rigidity ordering from cosmic-ray transport theory, consistent with standard turbulence-based interpretations of heliospheric diffusion. Also, the behavior of the radial part of the perpendicular MFP exhibits a flatter profile at higher

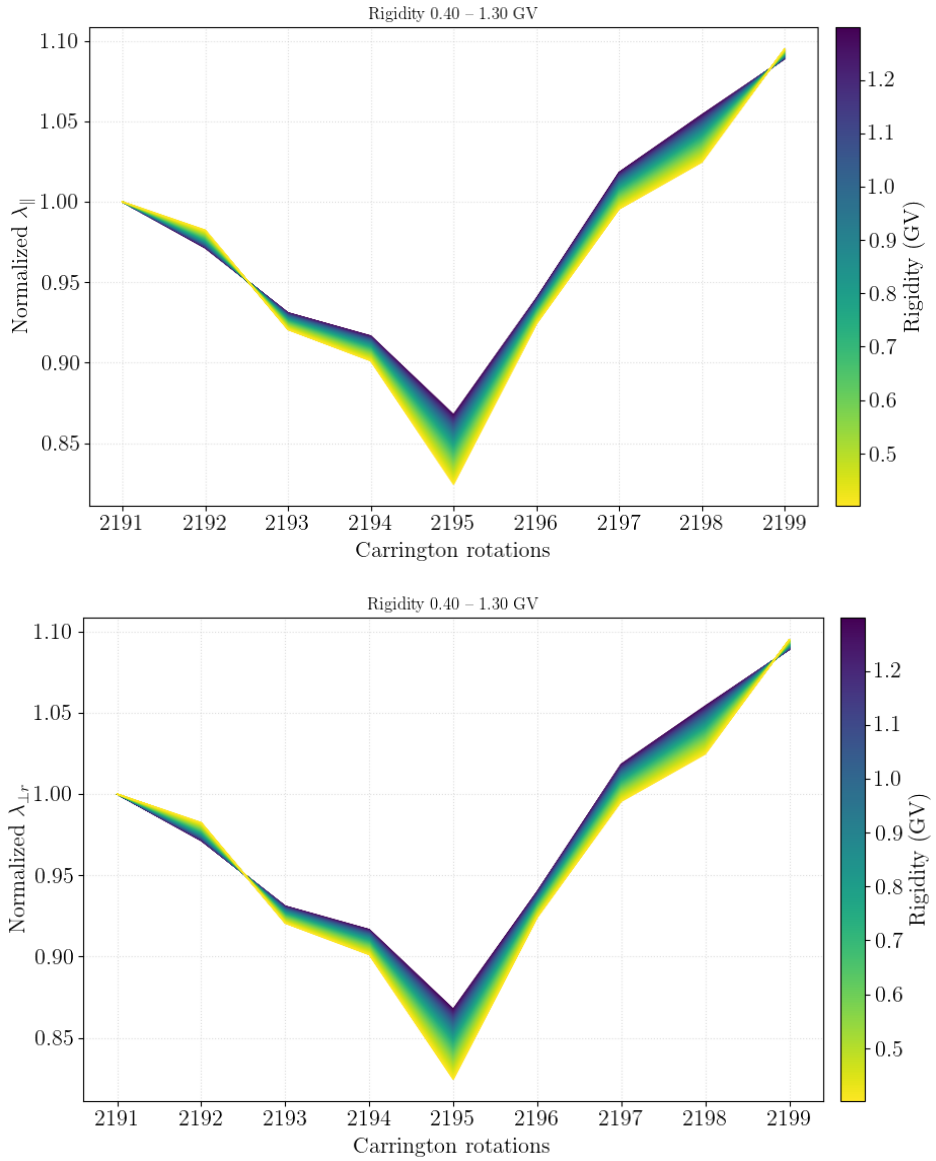


Figure 7. Time dependence in parallel ($\lambda_{\parallel}$; top) and perpendicular ($\lambda_{\perp r}$; bottom) MFPs of protons for rigidities of 0.40–1.30 GV, over the 2017 depression period CR2191–CR2199, normalized with respect to CR2191. These values are based on the parameterization of Model 2.

rigidities—another property that brings the solution closer in line with basic theory (e.g., N. E. Engelbrecht et al. 2022).

The results found here suggest that modeling $\kappa_{\perp}/\kappa_{\parallel}$ as varying in time may help to improve the results of other studies (e.g., X. Song et al. 2021; C. Corti 2023) and remove some physical inconsistencies (assuming there is a physical justification for changing the ratio in time, as there is for the 2017 GCR depression). We stress that this modification does not guarantee physical consistency in all circumstances, but offers a targeted and observationally supported adjustment for a specific class of modulation events. Its applicability to other periods and to fully time-dependent models (e.g., X. Song et al. 2021) remains an important topic for future investigation.

Acknowledgments

O.P.M.A. and D.M. acknowledge support from a Leverhulme Trust grant (RPG-2023-182). D.M. also acknowledges support from a Science and Technologies Facilities Council (STFC) grant (ST/Y001672/1) and a Personal Fellowship from the Royal Society of Edinburgh (ID: 4282). Results were obtained using the ARCHIE-WeSt High Performance Computer, www.archie-west.ac.uk, based at the University of Strathclyde.

ORCID iDs

O. P. M. Aslam https://orcid.org/0000-0001-9521-3874
D. MacTaggart https://orcid.org/0000-0003-2297-9312
M. S. Potgieter https://orcid.org/0000-0003-0793-7333
M. D. Ngobeni https://orcid.org/0000-0001-5844-3419
I. I. Ramokgaba https://orcid.org/0000-0002-0605-1306

References

Adriani, O., Barbarino, G. C., Bazilevskaya, G. A., et al. 2013, ApJ, 765, 91
Aguilar, M., Ali Cavasonza, L., Alpat, B., et al. 2018, PhRvL, 121, 051101
Aguilar, M., Ali Cavasonza, L., Ambrosi, G., et al. 2021a, PhR, 894, 1
Aguilar, M., Cavasonza, L. A., Ambrosi, G., et al. 2021b, PhRvL, 127, 271102

Aslam, O. P. M., MacTaggart, D., Battiston, R., Potgieter, M. S., & Ngobeni, M. D. 2025, ApJ, 981, 174
Aslam, O. P. M., Potgieter, M. S., Luo, X., & Ngobeni, M. D. 2023, ApJ, 953, 101
Bieber, J. W., & Matthaeus, W. H. 1991, ICRC, 3, 248
Bieber, J. W., Matthaeus, W. H., Shalchi, A., & Qin, G. 2004, GeoRL, 31, L10805
Bisschoff, D., Potgieter, M. S., & Aslam, O. P. M. 2019, ApJ, 878, 59
Burger, R. A., & Potgieter, M. S. 1989, ApJ, 339, 501
Burger, R. A., Potgieter, M. S., & Heber, B. 2000, JGR, 105, 27447
Cane, H. V. 2000, SSRv, 93, 55
Corti, C. 2023, ICRC, 444, 1283
Dumbović, M., Vrsnak, B., et al. 2022, A&A, 658, A187
Dumbović, M., et al. 2020, SoPh, 295, 104
Engelbrecht, N. E., Effenberger, F., Florinski, V., et al. 2022, SSRv, 218, 33
Ferreira, S. E. S., Potgieter, M. S., Burger, R. A., & Heber, B. 2000, JGR, 105, 18305
Ferreira, S. E. S., Potgieter, M. S., Moeketsi, D. M., Heber, B., & Fichtner, H. 2003, ApJ, 594, 552
Fisk, L. A. 1999, AdSpR, 23, 415
Forsyth, R. J., Balogh, A., Smith, E. J., Erdös, G., & McComas, D. J. 1996, JGR, 101, 395
Gleeson, L. J., & Axford, W. I. 1967, ApJL, 149, L115
Heber, B., & Potgieter, M. S. 2006, SSRv, 127, 117
Jokipii, J. R. 1966, ApJ, 146, 480
Jokipii, J. R., & Kóta, J. 1989, GeoRL, 16, 1
Jokipii, J. R., Levy, E. H., & Hubbard, W. B. 1977, ApJ, 213, 861
Jokipii, J. R., & Thomas, B. 1981, ApJ, 243, 1115
Kóta, J., & Jokipii, J. R. 1983, ApJ, 265, 573
Kóta, J., & Jokipii, J. R. 1995, ICRC, 4, 680
Langner, U. W., Potgieter, M. S., Fichtner, H., & Borrmann, T. 2006, ApJ, 640, 1119
Lockwood, J. A. 1971, SSRv, 12, 658
Luo, X., Potgieter, M. S., Zhang, M., & Shen, F. 2024, ApJ, 961, 21
Manuel, R., Ferreira, S. E. S., & Potgieter, M. S. 2015, ApJ, 799, 223
Martucci, M., Munini, R., Boezio, M., et al. 2018, ApJL, 854, L2
Matthaeus, W. H., Qin, G., Bieber, J. W., & Zank, G. P. 2003, ApJL, 590, L53
Moloto, K. D., & Engelbrecht, N. E. 2020, ApJ, 894, 121
Ngobeni, M. D., & Potgieter, M. S. 2011, AdSpR, 48, 300
Ngobeni, M. D., & Potgieter, M. S. 2015, AdSpR, 56, 1525
Ngobeni, M. D., Potgieter, M. S., Aslam, O. P. M., et al. 2022, AdSpR, 69, 2330
Ngobeni, M. D., Aslam, O. P. M., Bisschoff, D., et al. 2020, Ap&SS, 365, 182
Parker, E. N. 1958, PhRv, 110, 1445
Parker, E. N. 1965, P&SS, 13, 9
Pei, C., Bieber, J. W., Breech, B., et al. 2010, JGRA, 115, A03103
Potgieter, M. S. 1998, SSRv, 83, 147
Potgieter, M. S. 2000, JGR, 105, 18295
Potgieter, M. S. 2013a, LRSP, 10, 3
Potgieter, M. S. 2013b, SSRv, 176, 165
Potgieter, M. S. 2017, AdSpR, 60, 848
Potgieter, M. S., Aslam, O. P. M., Bisschoff, D., & Ngobeni, D. 2021, Physi, 3, 1190
Potgieter, M. S., & Haasbroek, L. J. 1993, ICRC, 3, 457
Potgieter, M. S., & Moraal, H. 1985, ApJ, 294, 425
Potgieter, M. S., Vos, E. E., Boezio, M., et al. 2014, SoPh, 289, 391
Potgieter, M. S., Vos, E. E., Munini, R., Boezio, M., & Di Felice, V. 2015, ApJ, 810, 141
Raath, J. L., Potgieter, M. S., Strauss, R. D., & Kopp, A. 2016, AdSpR, 57, 1965
Rankin, J. S., Bindi, V., Bykov, A. M., et al. 2022, SSRv, 218, 42
Schlickeiser, R. 1988, JGR, 93, 2725
Shalchi, A. 2006, A&A, 453, L43
Shalchi, A. 2009, Nonlinear Cosmic Ray Diffusion Theories, 362 (Springer)
Shalchi, A. 2010, ApJL, 720, L127
Shalchi, A., Bieber, J. W., & Matthaeus, W. H. 2004, ApJ, 615, 805
Smith, C. W., & Bieber, J. W. 1991, ApJ, 370, 435
Song, X., Luo, X., Potgieter, M. S., Liu, X., & Geng, Z. 2021, ApJS, 257, 48
Tan, B., Zhang, Y., Huang, J., & Ji, K. 2025, ApJL, 979, L16
Wibberenz, G., Le Roux, J. A., Potgieter, M. S., & Bieber, J. W. 1998, SSRv, 83, 309